Influence of double-electron transitions on the EXAFS L edges of rare-earth systems

Jesús Chaboy, Augusto Marcelli, and Trevor A. Tyson*
Istituto Nazionale di Fisica Nucleare, Casella Postale, Laboratori Nazionali di Frascati, 13, 00044 Frascati, Italy
(Received 26 July 1993)

This work presents an x-ray-absorption study at the L edges of several rare-earth compounds. In both L_1-edge and L_3-edge spectra, anomalous features are clearly detected in the EXAFS region and have been associated with the creation of $2s4d$ and $2p4d$ double-core hole states, respectively. Comparison of theoretical calculations with the experiments are carried out using the results of explicit computation of cross sections for the allowed mainline (L edge) and double-electron ($LN_{4,5}$ edges) which identify the transitions expected to be observable. In addition, the excitation energies of all of these allowed transitions are given. The influence of multielectron transitions on the EXAFS data analysis is discussed for several rare-earth-based systems. An estimate of the error introduced by neglecting the presence of double-electron transitions on coordination numbers and bond distances is given, based on these experimental data.

I. INTRODUCTION

In recent years substantial progress has been made in the field of x-ray-absorption spectroscopy (XAS) strongly connected to both the advent of high intensity synchrotron radiation sources and significant developments in theoretical models. However, most of these models have been developed in the framework of one-electron theory which neglects multielectron excitations in which two or more electrons may be simultaneously excited. These many-electron processes induced by photon impact epitomize the breakdown of single-electron models providing very valuable information on electron correlation and excitation dynamics. This possibility broadened the range of experimental probes which could be used to study multiple-electron excitations, as heavy-ion–atom collisions,[1] Auger,[2,3] electron capture,[4] x-ray emission,[5–8] x-ray photoemission,[9,10] and charged-ion spectra.[11,12]

The existence of multielectron transitions was first observed in ionization by electron impact experiments.[13–15] However, the first experimental evidence of multielectron excitation in the x-ray-absorption spectra by photon impact were found in argon by Bonnelle and Wuilleumier[16] and Schnopper,[17] and in helium by Madden and Codling[18] in the mid-1960s. Because of their fundamental interest in developing atomic structure models, the first multielectron investigations in the x-ray-absorption spectra were carried out on gases such as Ne,[19–23] Ar,[24–26] Kr,[27–32] and Xe,[33–35] which exhibit no extended x-ray-absorption fine structure (EXAFS) hampering the weak features of the spectrum associated with the small cross sections involved in the multielectron process. Indeed, first detections of such processes in the absorption spectra of solid targets as transition metals[36–41] and rare-earth compounds[41–44] were not reported until the early 1980s and, even now, there is a strong controversy concerning the reliability of these observations for transition-metal compounds.[45]

Beyond the basic atomic physics interest, the study of multielectron excitations in XAS has received renewed attention due to its possible impact on the extraction of structural information from EXAFS spectra. The identification of these features close to the absorption edge, i.e., in the x-ray-appearance near-edge-structure (XANES) region, is rather complicated due to the superposition of complex electronic excitations and multiple-scattering effects.[46,47] However, the complexity of the x-ray-absorption spectrum is reduced as the photoelectron energy increases in such a way that in the EXAFS region the spectra can be interpreted with high accuracy in terms of a single-electron theory and with a finite number of multiple-scattering paths. The detection of features arising from multielectron excitations in EXAFS of crystalline systems is made difficult by the presence of a large signal due to the scattering processes of the photoelectron with neighboring atoms. Consequently, they have been easily identified only in disordered systems in which the intensity associated with these excitations is comparable with the amplitude of the EXAFS oscillation.[48–55]

In this way, several investigations of the x-ray-absorption fine structure of rare-earth-based materials have reported the existence of several anomalous peaks far above the main white line, $k \approx 6$ Å^{-1}.[49,50] These features located in the EXAFS region were attributed to simultaneous excitation of $2s$ and $4d$ electrons in the case of the L_1 edge and to the excitation of $2p$ and $4d$ electrons in the case of the L_2 and L_3 edges. This identification was made on the grounds of the excitation energy of the $4d$ level in the $Z+1$ approximation that leads to a discrepancy of about 1 Ry with respect to the observed values. Moreover, no criteria for the assignment of the final state configurations involved in the process were given.

The presence of multielectron transitions in the EXAFS spectra influences the structural analysis by introducing unphysical structures at low R values in the Fourier transform of the EXAFS spectra and modifies its intensity. As a consequence, the structural analysis is contaminated resulting in a non-negligible error in both the coordination numbers (between 5% and 10%) and

interatomic distances extracted.[48]

These experimental findings led to the proposition of several data reduction methods to identify multielectron excitations in the EXAFS region, particularly in the case of crystalline systems where the double-excitation features are hidden by the XAFS structures.[56,57] However, both procedures are rather complicated and have so far led only to the identification of the energy position of several multielectron transitions without the determination of their shape.

The main goal of this investigation is the identification of multielectron excitations in the absorption spectra at the L edges of rare-earth-based systems. The determination of their shape leads us to a deeper insight into the nature of these transitions, whereas that of their intensity determination provides a direct way to assess the influence on the EXAFS structural analysis. We report the experimental EXAFS spectra for several rare-earth-doped silica gels showing double-electron features at both the L_3 and L_1 edges. The atomic nature of these multielectron excitations has been investigated in the case of rare-earth-doped silica glasses because the lack of long-range crystalline order makes possible an easier identification of the $LN_{4,5}$ double excitation superimposed on the EXAFS signal.

We have performed theoretical computation of cross sections for the allowed main line (L edge) and double-electron line ($LN_{4,5}$ edges) in the case of rare-earth atoms. The calculations were carried out for all the possible final states allowed showing which transitions are expected to be observable. The model is briefly described and a summary of the results is given. Finally, the application of these calculations to the experimental spectra is presented. The influence of the double-electron transitions to the structural analysis is also discussed for the case of amorphous and crystalline RM_2H_x systems (R=rare earth, M=transition metal).

II. EXPERIMENTAL SETUP AND DATA ANALYSIS

Experiments were carried out at the National Laboratory for High Energy Physics (KEK). The absorption spectra at the L edges of rare earths were recorded on beam line 7C at the Photon Factory.[58] The storage ring was operated with a positron energy of 2.5 GeV and a stored current of about 300 mA.

The beam line 7C was equipped with a Si(111) fixed-exit-beam double-crystal monochromator which provides also sagittal focusing of the synchrotron radiation. The allowed energy range is between 4 and 15 keV. Due to the energy of the storage ring, harmonic content is not negligible and its rejection is a crucial problem for XAS data. The beam line is equipped with a pair of quartz uncoated mirrors to reject higher harmonics at low energy whereas harmonic rejection at higher energy is achieved by detuning of the two parallel and independent crystals of the monochromator from the Bragg angle. During the measurements, to obtain total harmonics rejection, a critical angle of 4.7 mrad was set when working at energies less than 7 keV whereas a detuning of the crystals between 40% and 60% was applied at higher energies.

All the measurements were carried out at room temperature in the transmission mode. Both x rays incident on the sample and transmitted through it were monitored with two independent ionization chambers with a N_2-Ar flowing gas mixture optimized for each energy range. Silica-gel samples were provided by O. Gzowski and the details of the preparation are published elsewhere.[59] For the absorption measurements the gel samples were prepared in a single homogeneous layer of material obtained starting from a thick slab (1 mm) finely reduced to obtain an absorption jump of around 1. The thickness and homogeneity of the samples were tested in advance by using a rotating anode laboratory EXAFS spectrometer.

RNi_2 and their hydride derivatives were provided by J.-Y. Lee. The preparation details and the characterization of samples have been previously reported.[60,61] For the absorption experiments samples were prepared starting from homogeneous-size powders spread on a kapton tape. The thickness and homogeneity of the samples were optimized in order to obtain the best signal to noise ratio; thus two layers of powder material were used giving a total $\Delta\mu x$ of 0.5.

EXAFS signals were extracted from the raw spectra by using the standard techniques. The background contribution from previous edges $\mu_B(E)$ was approximated according to the Victoreen rule[62] $\mu_B(E) = A/E^3 + B/E^4$ and subtracted from the experimental spectrum $\mu(E)$, after which, the atomiclike term $\mu_0(E)$ was found by a cubic-spline approximation and the EXAFS signal $\chi(k)$ was determined as $\chi(k) = (\mu - \mu_B - \mu_0)/\mu_0$, where the photoelectron wave vector k is defined by $k = (2m/\hbar^2)\sqrt{(E - E_0)}$. The energy origin E_0, corresponding to the continuum threshold, was defined to be at the inflection point of the absorption edge for all the systems studied. The EXAFS signals were Fourier transformed (FT) by using in all the cases the same Gaussian window, e^{-Ak^2} with A=0.05, centered at the midpoint of the data range. Note that the phase correction was not included in the FT; therefore the peaks positions are shifted from their true values.

III. RESULTS AND DISCUSSION

The L_3 absorption spectra of rare-earth atoms in the different rare-earth gels (R=Nd, Pr, Eu, Gd, Dy, Er), reported in Fig. 1, are characterized by the same oscillating behavior revealing the existence of low local order around the rare-earth site. Indeed, the EXAFS structure is formed by a near single-frequency oscillation indicating that only an ordered coordination shell, formed by oxygen atoms,[59] is seen from the rare-earth site. Then, the unique expected difference in the EXAFS region in going from compound to compound is associated with the change of frequency of the different oscillations that contribute to the full spectrum, reflecting the small change of the R-O bond length across the series. This trend clearly appears in Fig. 1, where the extracted EXAFS signals at the L_3 edge of the rare earth for the different gels is reported. However, the EXAFS signals also exhibit large differences in the region between 6 and 7

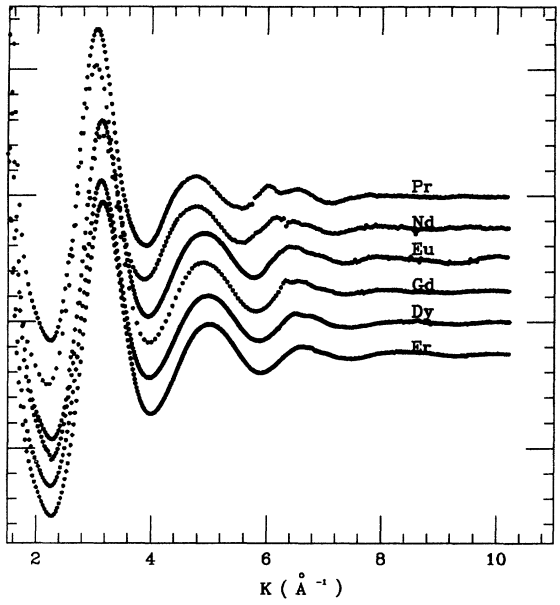

FIG. 1. Comparison of the EXAFS spectra at the R L_3 edge in several rare-earth-doped silica-gel compounds (R= Pr, Nd, Eu, Gd, Dy, and Er). The EXAFS signal has been extracted from the raw absorption spectra following conventional methods (see text).

$Å^{-1}$. In this region, the Pr-based gel presents a double-peak structure and the low-energy component collapses as Z (atomic number) increases in such a manner that for Eu there is a single peak. However, moving from a Gd- to Er-based gel, the structure becomes again a double peaked but now it seems that low-energy profile of the feature in the case of the Pr gel has been crossed to the high-energy region.

The fact that the energy location of these features varies as a function of the rare earth whereas the other EXAFS structures remain unchanged strongly suggests that they are due to some multielectron process. Therefore, when looking at the promotion energy for a second electron, one finds in the $Z+1$ approximation that the energy roughly corresponds to the excitation of a secondary $4d$ electron. Applying this approximation means that we consider the $2p$ hole to be fully screened prior to the second excitation taking place. Then, in the fully relaxed state the atomic configuration would correspond to that of the next atom in the periodic table. However, this is a crude approximation as indicated by the disagreement between the experimental and predicted energies ($\approx 15\%$ for rare earths; see Tables I and II), and no information about the final states involved in the multielectron transition can be inferred.

To demonstrate that this behavior is associated to the existence of a $2p4d \rightarrow (5d)^2$ transition we have applied the result of the explicit computation of the relative cross sections for bound-state double-electron $LN_{4,5}$-edge transitions.[63] These calculations were performed by using a many-body perturbation model that takes explicitly into account final state relaxation.[64] Radial wave functions were obtained, for the ground state and excited state, using a spherical model of the atom (Hartree-Fock-Slater). If the single-photon absorption creates two holes (double excitation), the resulting final states are composed of the set of four-particle (two holes and two electrons) Slater determinants allowed by the exclusion principle. These final states are in general a set of ^1P multiple states separated in energy by the perturbations introduced by the residual Coulomb interaction and the molecular corrections to the mean potential. The resulting cross section for a specific state depends on both the monopole and the dipole radial matrix elements of the ground and excited states. Because of the large core-hole width for a $4d$ electron,[65] the multiplet splitting is not observable at this energy; hence all of the ^1P states were summed for a given electron configuration.

For the EXAFS analysis we are interested in determining just how large the bound-state features are relative to the EXAFS amplitude; hence we compute the ratio of the double-electron cross section to that of the main excitation. This is made for all the possible final states allowed in order to show which transitions are expected to be observable. Table I shows the result of the calculations in the case of $L_{2,3}N_{4,5}$ edges for several rare earths, R= La, Ce, Pr, Nd, Eu, Gd, Dy, and Er. Moreover, the same calculations performed in the case of an L_1 excitation, i.e., $L_1N_{4,5}$ edges, are reported in Table II. To perform the comparison between the calculated and experimental double-electron signals we have proceeded as follows: As our calculations directly report the ratio between the single- and double-excitation cross sections, we extract from the experiment the area of the main line that corresponds to the $2p \rightarrow 5d$ transition, in the case of an L_3 edge or $2s \rightarrow 6p$ for an L_1 edge. To do this, we apply a deconvolution model to the experimental data which uses an arctangent function to describe the transitions into the continuum states and a Lorentzian function to take account of the $5d(6p)$ states.[66] The deconvolution process was performed using a least squares fitting procedure to fit the normalized spectra to the expression

$$F(E) = B_0 + B_1E + \frac{(\frac{\Gamma}{2})^2 A_1}{(E-E_1)^2 + (\frac{\Gamma}{2})^2} + \left\{ \frac{1}{2} + \frac{1}{\pi} \arctan\left[\frac{E-(E_1+\delta)}{\frac{\Gamma}{2}} \right] \right\}, \quad (1)$$

where E is the photon energy and E_1 is the first accessible $5d$ state. Γ is the core-hole lifetime for the considered transition and δ is the shift between the onset of the continuum and bound-state transitions. Finally, B_0 and B_1 are the coefficients of a linear background while A_1 describes the intensity of the transition. Once the area for the main transition has been determined, we generate the multielectron transition resonance by multiplying the area by the calculated ratio between the double- and single-electron cross sections, $\bar{\sigma}_D^0/\bar{\sigma}_S$, and by including the core-hole lifetime that corresponds to the additional $4d$ excited electron.

Figure 2 shows the experimental EXAFS spectra at the L_3 edge of the rare earth for several R-based silica gels

(R= Pr, Nd, Eu, Gd, Dy, and Er) in the region where the double-excitation feature has been identified. The calculated multielectron resonances have been included above the experimental signals. According to the *ab-initio* calculations reported in Table I, the main double-excitation channel corresponds to the $2p4d \rightarrow (5d)^2$ transition, with negligible contribution from other channels. In particular, the cross section for the transition to a $5d6d$ final state is reduced by a factor greater than 10 as compared with that involving a $5d5d$ final state, as shown in Ta-

TABLE I. $L_{2,3}N_{4,5}$-edge transition intensities and excitation energies.[a]

Atom	Transition	$\overline{\sigma}_D^0$	$\Delta\omega$	$\overline{\sigma}_D^0/\overline{\sigma}_S(\%)$	$\Delta\omega(Z+1)$
Z=57	$5d,5d \longleftarrow 2p,4d$	4.867×10^{-3}	9.048	2.16	8.01
	$5d,6d \longleftarrow 2p,4d$	3.600×10^{-4}	9.617	0.16	
	$7s,5d \longleftarrow 2p,4d$	7.851×10^{-6}	9.580	3.49×10^{-3}	
	$7s,6d \longleftarrow 2p,4d$	8.010×10^{-7}	9.580	3.55×10^{-4}	
	$6p,4f \longleftarrow 2p,4d$	2.778×10^{-7}	8.147	2.78×10^{-4}	
	$6p,6p \longleftarrow 2p,4d$	4.544×10^{-9}	9.961	2.65×10^{-6}	
Z=58	$5d,5d \longleftarrow 2p,4d$	2.940×10^{-3}	8.956	1.66	8.46
	$5d,6d \longleftarrow 2p,4d$	2.614×10^{-4}	9.445	0.15	
	$7s,5d \longleftarrow 2p,4d$	5.620×10^{-6}	9.412	3.18×10^{-3}	
	$7s,6d \longleftarrow 2p,4d$	6.502×10^{-7}	10.173	3.68×10^{-4}	
	$6p,4f \longleftarrow 2p,4d$	3.652×10^{-7}	8.346	2.06×10^{-4}	
	$6p,6p \longleftarrow 2p,4d$	3.710×10^{-9}	9.694	2.10×10^{-6}	
Z=59	$5d,5d \longleftarrow 2p,4d$	2.402×10^{-3}	9.402	1.40	8.86
	$5d,6d \longleftarrow 2p,4d$	2.091×10^{-4}	9.885	0.12	
	$7s,5d \longleftarrow 2p,4d$	4.570×10^{-6}	9.849	2.67×10^{-3}	
	$7s,6d \longleftarrow 2p,4d$	5.281×10^{-7}	10.62	3.08×10^{-4}	
	$6p,4f \longleftarrow 2p,4d$	3.373×10^{-7}	8.733	1.97×10^{-4}	
	$6p,6p \longleftarrow 2p,4d$	3.348×10^{-9}	10.137	1.95×10^{-6}	
Z=60	$5d,5d \longleftarrow 2p,4d$	1.991×10^{-3}	9.845	1.20	8.82
	$5d,6d \longleftarrow 2p,4d$	1.700×10^{-4}	10.330	0.10	
	$7s,5d \longleftarrow 2p,4d$	3.779×10^{-6}	10.289	2.28×10^{-3}	
	$7s,6d \longleftarrow 2p,4d$	4.359×10^{-7}	11.065	2.63×10^{-4}	
	$6p,4f \longleftarrow 2p,4d$	3.125×10^{-7}	9.111	1.89×10^{-4}	
	$6p,6p \longleftarrow 2p,4d$	3.028×10^{-9}	10.576	1.83×10^{-6}	
Z=63	$5d,5d \longleftarrow 2p,4d$	1.191×10^{-3}	11.179	0.802	9.39
	$5d,6d \longleftarrow 2p,4d$	0.968×10^{-4}	11.652	0.065	
	$7s,5d \longleftarrow 2p,4d$	2.264×10^{-6}	11.611	1.53×10^{-3}	
	$7s,6d \longleftarrow 2p,4d$	2.597×10^{-7}	12.392	1.75×10^{-4}	
	$6p,4f \longleftarrow 2p,4d$	2.498×10^{-7}	10.288	1.68×10^{-4}	
	$6p,6p \longleftarrow 2p,4d$	2.248×10^{-9}	11.888	1.51×10^{-6}	
Z=64	$5d,5d \longleftarrow 2p,4d$	1.549×10^{-3}	12.185	0.838	11.066
	$5d,6d \longleftarrow 2p,4d$	0.985×10^{-4}	12.749	0.053	
	$7s,5d \longleftarrow 2p,4d$	2.440×10^{-6}	12.704	1.32×10^{-3}	
	$7s,6d \longleftarrow 2p,4d$	2.440×10^{-7}	13.596	1.32×10^{-4}	
	$6p,4f \longleftarrow 2p,4d$	2.525×10^{-7}	10.847	1.37×10^{-4}	
	$6p,6p \longleftarrow 2p,4d$	2.287×10^{-9}	13.069	1.24×10^{-6}	
Z=66	$5d,5d \longleftarrow 2p,4d$	7.473×10^{-4}	12.523	0.567	11.765
	$5d,6d \longleftarrow 2p,4d$	5.847×10^{-5}	12.984	0.044	
	$7s,5d \longleftarrow 2p,4d$	1.440×10^{-6}	12.940	1.09×10^{-3}	
	$7s,6d \longleftarrow 2p,4d$	1.643×10^{-7}	13.719	1.25×10^{-4}	
	$6p,4f \longleftarrow 2p,4d$	2.022×10^{-7}	11.466	1.54×10^{-4}	
	$6p,6p \longleftarrow 2p,4d$	1.689×10^{-9}	13.200	1.28×10^{-6}	
Z=68	$5d,5d \longleftarrow 2p,4d$	5.576×10^{-4}	13.438	0.460	12.90
	$5d,6d \longleftarrow 2p,4d$	4.279×10^{-5}	13.894	0.035	
	$7s,5d \longleftarrow 2p,4d$	1.090×10^{-6}	13.846	0.90×10^{-3}	
	$7s,6d \longleftarrow 2p,4d$	1.241×10^{-7}	14.618	1.02×10^{-4}	
	$6p,4f \longleftarrow 2p,4d$	1.768×10^{-7}	12.342	1.46×10^{-4}	
	$6p,6p \longleftarrow 2p,4d$	1.407×10^{-9}	14.091	1.16×10^{-6}	

[a]All lengths are in Bohr radii (0.5292 Å), energies are in rydbergs (13.61 eV), and the cross section strengths are given in units of megabarn rydbergs. The excitation energy given for each transition $\Delta\omega$ is relative to the corresponding single-hole state $5d \longleftarrow 2p$. $\overline{\sigma}_D^0$ and $\overline{\sigma}_S$ represent the calculated cross section strengths for the double- and single-electron absorption processes, respectively.

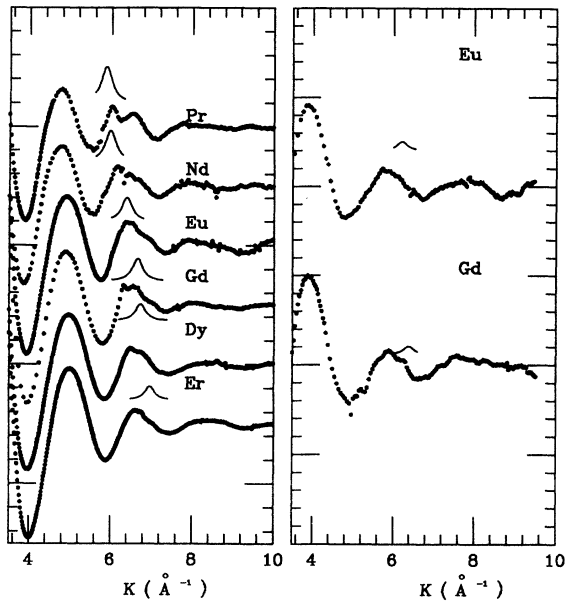

FIG. 2. The dotted lines correspond to the EXAFS spectra at the R L_3 (left panel) and L_1 edges (right panel) for the different rare-earth-doped silica-gel compounds studied. The EXAFS signals are plotted in a narrow k window to make evident the features identified as multielectron transitions. The solid line represents the simulation for double-electron resonances of type $2p4d \rightarrow (5d)^2$ and $2s4d \rightarrow 6p5d$ for the L_3 and L_1 edges, respectively.

ble I. The same class of comparison is shown in Fig. 2 for the case of the rare-earth L_1-edge EXAFS spectra in the same materials. In this case the intensity of the double-electron resonance, corresponding to a $2s4d \rightarrow 6p5d$ transition (see Table II), is very weak as compared with that of the L_3 EXAFS spectra. In both cases, the agreement between the calculated energy position and intensity of the double-electron features and the experimental ones can be considered very good. As shown in Fig. 2, the anomalous behavior of the EXAFS resonance centered at $k \approx 6.5$ Å^{-1} is fully reproduced by taking into account the theoretical calculation for the $LN_{4,5}$-edge multielectron transitions.

It is important to underline that the good agreement obtained between the experimental and calculated signals is connected to the quality of the experimental data. In fact, being interested in extracting from the experiment the intensity of the main transition, one has to be careful with harmonics rejection of the photon beam because its presence leads to a strong unphysical reduction of the XAS signal. Figure 3 reports the comparison between the Nd L_3-edge spectra taken with mirrors (full harmonics rejection) and with partial rejection obtained by detuning the monochromator (60%). In the last case, a high harmonics content is still present in the incident beam yielding to a strong reduction of the main line intensity. The use of this last spectrum yields a reduction of the calculated double-electron transition of about one-

TABLE II. $L_1N_{4,5}$-edge transition intensities and excitation energies.[a]

Atom	Transition	$\bar{\sigma}_D^0$	$\Delta\omega$	$\bar{\sigma}_D^0/\bar{\sigma}_S(\%)$	$\Delta\omega(Z+1)$
Z=57	$6p,5d \longleftarrow 2s,4d$	1.80×10^{-4}	9.133	2.45	8.01
	$7s,6p \longleftarrow 2s,4d$	1.108×10^{-10}	9.861	2.42×10^{-6}	
	$7s,4f \longleftarrow 2s,4d$	9.163×10^{-8}	7.975	9.34×10^{-4}	
Z=58	$6p,5d \longleftarrow 2s,4d$	1.558×10^{-4}	9.041	1.79	8.46
	$7s,6p \longleftarrow 2s,4d$	1.698×10^{-10}	9.673	1.94×10^{-6}	
	$7s,4f \longleftarrow 2s,4d$	1.309×10^{-8}	10.471	1.50×10^{-4}	
Z=59	$6p,5d \longleftarrow 2s,4d$	1.150×10^{-4}	9.481	1.36	8.86
	$7s,6p \longleftarrow 2s,4d$	1.532×10^{-10}	10.114	1.81×10^{-6}	
	$7s,4f \longleftarrow 2s,4d$	1.247×10^{-8}	8.636	1.47×10^{-4}	
Z=60	$6p,5d \longleftarrow 2s,4d$	1.057×10^{-4}	9.924	1.29	8.82
	$7s,6p \longleftarrow 2s,4d$	1.386×10^{-10}	10.557	1.69×10^{-6}	
	$7s,4f \longleftarrow 2s,4d$	1.156×10^{-8}	9.017	1.41×10^{-4}	
Z=63	$6p,5d \longleftarrow 2s,4d$	6.389×10^{-5}	11.253	0.847	9.39
	$7s,6p \longleftarrow 2s,4d$	1.028×10^{-10}	11.881	1.363×10^{-6}	
	$7s,4f \longleftarrow 2s,4d$	0.924×10^{-8}	10.206	1.23×10^{-4}	
Z=64	$6p,5d \longleftarrow 2s,4d$	7.332×10^{-5}	12.259	0.893	11.066
	$7s,6p \longleftarrow 2s,4d$	9.941×10^{-11}	12.765	1.21×10^{-6}	
	$7s,4f \longleftarrow 2s,4d$	0.874×10^{-8}	10.765	1.09×10^{-4}	
Z=66	$6p,5d \longleftarrow 2s,4d$	4.107×10^{-5}	12.602	0.593	11.765
	$7s,6p \longleftarrow 2s,4d$	7.733×10^{-11}	13.217	1.12×10^{-6}	
	$7s,4f \longleftarrow 2s,4d$	7.505×10^{-9}	11.443	1.08×10^{-4}	
Z=68	$6p,5d \longleftarrow 2s,4d$	3.122×10^{-5}	13.517	0.476	12.90
	$7s,6p \longleftarrow 2s,4d$	6.452×10^{-11}	14.119	9.835×10^{-7}	
	$7s,4f \longleftarrow 2s,4d$	6.583×10^{-9}	12.2946	1.00×10^{-4}	

[a]All lengths are in Bohr radii (0.5292 Å) and all energies are in rydbergs (13.61 eV). The cross section strengths are given in units of megabarns rydbergs. The excitation energy given for each transition $\Delta\omega$ is relative to the corresponding single-hole state; e.g., it is above the $6p \longleftarrow 2s$ configuration. $\bar{\sigma}_D^0$ and $\bar{\sigma}_S$ represent the calculated cross section strength for the double- and single-electron absorption processes, respectively.

half of the experimentally observed.

The improvement of the calculations performed as well as the comparison method proposed has allowed us to successfully extend the study of double-electron transitions to more complicated systems such as those in which Ce presents mixed valence behavior: $Ce(NO_3)_4$. Due to the existence of two configurations in the initial state, $4f^n$ and $4f^{n+1}$, the main line at the L_3 edge shows a characteristic double-peak profile. In this case, the deconvolution procedure must be extended to include two arctangent and two Lorentzian functions to take account of the two final state configurations present. Hence, we have changed the deconvolution formula of expression (1) to

$$F(E) = B_0 + B_1 E + \frac{(\frac{\Gamma}{2})^2 A_1}{(E-E_1)^2 + (\frac{\Gamma}{2})^2} + \frac{(\frac{\Gamma}{2})^2 A_2}{(E-E_1)^2 + (\frac{\Gamma}{2})^2} + \frac{A_1}{A_1 + A_2}\left\{\frac{1}{2} + \frac{1}{\pi}\arctan\left[\frac{E-(E_1+\delta)}{\frac{\Gamma}{2}}\right]\right\} + \left\{1 - \frac{A_1}{A_1 + A_2}\right\}\left\{\frac{1}{2} + \frac{1}{\pi}\arctan\left[\frac{E-(E_2+\delta)}{\frac{\Gamma}{2}}\right]\right\}, \quad (2)$$

where now E_1 and E_2 are, respectively, the first accessible $5d$ states in $4f^{n+1}$ and $4f^n$ configurations and A_1 and A_2 describe the relative weight of the two configurations. The deconvolution of the L_3 absorption edge of cerium for $Ce(NO_3)_4$ is given in Fig. 4.

In this case, the existence of two different double-electron resonances can be expected in the EXAFS spectra separated by 0.66 Ry (9 eV), corresponding to the double main line shift, and with a relative intensity that reproduces the weight of each configuration in the initial state. Figure 5 shows the EXAFS spectra at the L_3 and L_1 edges of cerium in the case of the $Ce(NO_3)_4$ system. We have included the result of the calculations for the $2p4d \rightarrow (5d)^2$ and $2s4d \rightarrow 6p5d$ transitions (Tables I and II) obtained by applying the deconvolution process according to Eq. (2).

The energy location of the resultant transitions matches the only region of both the L_3 and L_1 EXAFS spectra where the application of the "π approach"[56] shows a strong disagreement. This simple method of comparison between L_3 and L_1 spectra considers the existence of a π shift between the L_3 and the L_1 EXAFS phases. Within its intrinsic limits (accurate discussion is given in Ref. 56) this approximation leads to a qualitative correspondence between maxima and minima of the L_3 and L_1 EXAFS signals. From Fig. 5 it is inferred that only after the subtraction of the double-excitation

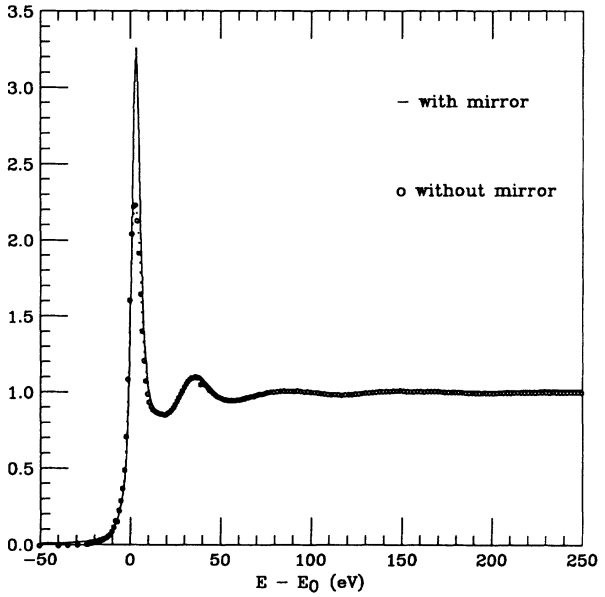

FIG. 3. Comparison between the normalized absorption spectra at the Nd L_3 edge for Nd-doped silica gel, recorded at Photon Factory Beamline 7C using a double mirror system to achieve a full harmonic rejection (solid line) or by simply detuning (60%) the cyrstals of the monochromator (dotted line).

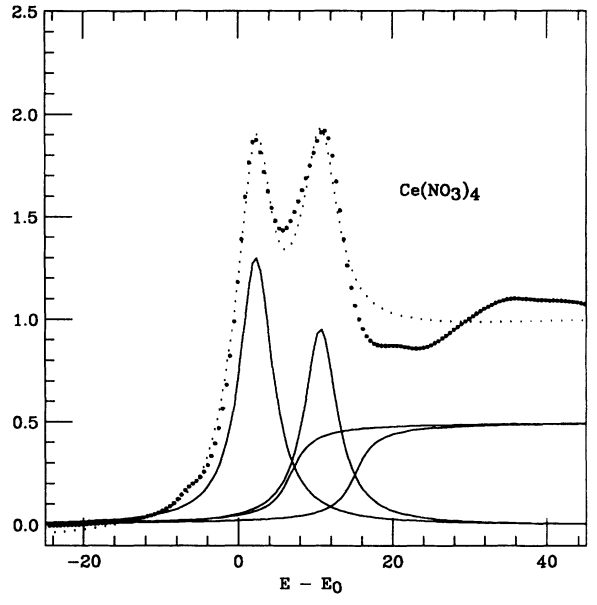

FIG. 4. Deconvolution of the Ce L_3-edge absorption spectrum in the mixed valence system $Ce(NO_3)_4$. Due to the existence of two configurations in the initial state, $4f^n$ and $4f^{n+1}$, the white line at the L_3 edge shows a characteristic double-peak profile, shifted by 0.66 Ry (9 eV). The deconvolution has been performed including two arctangent and two Lorentzian functions according to expression (2) in the text.

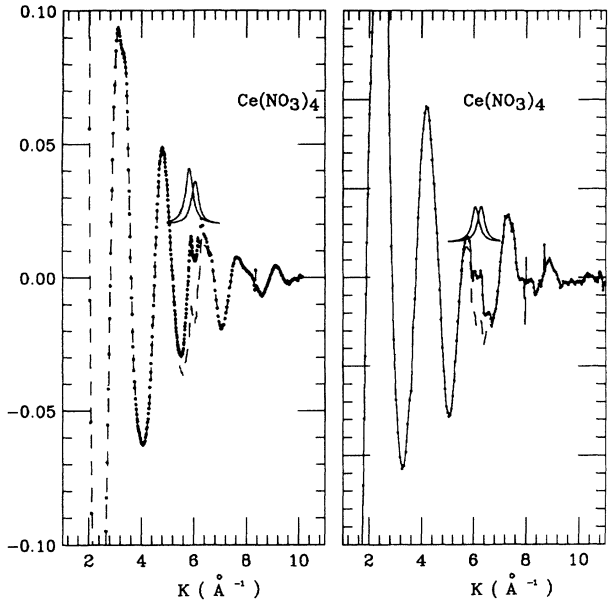

FIG. 5. EXAFS spectra at the L_3 and L_1 edges of cerium in the case of the $Ce(NO_3)_4$ system. We have included the result of the calculations for the $2p4d \rightarrow (5d)^2$ and $2s4d \rightarrow 6p5d$ transitions (Tables I and II) obtained by applying the deconvolution process.

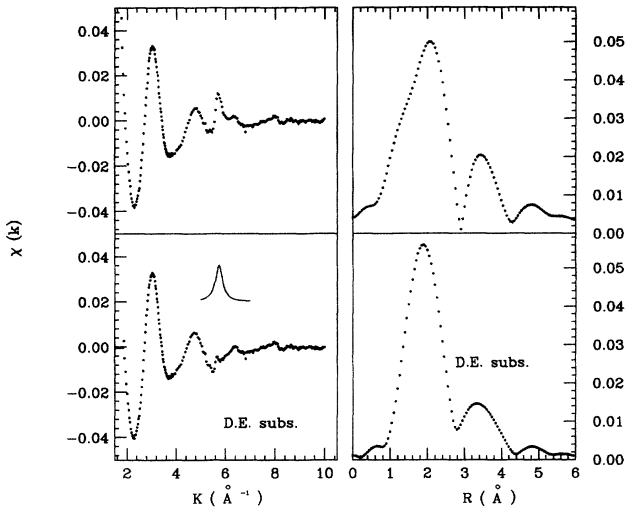

FIG. 6. Comparison between the La L_3-edge EXAFS spectra in the highly disordered system $LaNi_2H_x$: In the bottom, the resonance due to the $2p4d \rightarrow (5d)^2$ transition has been subtracted from the raw spectrum. In the right panel the same comparison is shown for the Fourier transforms of the EXAFS spectra.

resonances does one obtain a better correspondence between the EXAFS oscillations at the two edges obtained by applying the π approach. These experimental results reveal the line shape of the double excitation to be, within the experimental resolution, a single peak indicating that the bound to bound transitions are the dominant process. The presence of competing shakeoff transitions is without doubt, but experiments report that their intensity is negligible at the energy ranges involved in our investigation. In particular the presence of shake-off transitions would be evidencied by slope changes of the absorption spectra,[35] which have not been observed in the present investigation. The same result has been found, to our knowledge, in all the works made up on the L edges of rare earths[49–55] being in good agreement with theoretical calculations.[63]

Finally we discuss the implications of the double-electron features relative to the EXAFS data analysis in both crystalline and amorphous rare-earth systems. Figure 6 reports the La L_3-edge EXAFS spectrum of the $LaNi_2$ hydride derivative. After the hydrogen absorption this system loses long-range crystalline order but, as shown in Fig. 6, a well-defined local order remains around the rare-earth site. The EXAFS spectrum is characterized by the existence of a strong resonance located at 5.8 $Å^{-1}$ that we ascribe to the existence of a $2p4d \rightarrow (5d)^2$ double-electron transition. When proceeding to the conventional data analysis by performing the Fourier transform of the spectrum we obtain a very broad peak at low R that makes it impossible to extract any structural information. However, if we subtract the calculated multi-electron resonance the Fourier transform obtained yields well-defined peaks each one corresponding to the different coordination shells around the La site. This is shown in Fig. 6 where Fourier transforms were performed in the range 1.8–7 $Å^{-1}$ on the k-weighted EXAFS spectra by imposing a Gaussian window centered at the midpoint of the data range. We have to underline that attempts to fit the backtransformed signal to the expected La-Ni scattering paths were unsuccessful prior to subtraction of the double-excitation feature because the signal was strongly distorted.

The same class of analysis has been performed in the case of crystalline systems. Figure 7 reports the Ce L_3-edge EXAFS spectra of $CeFe_2$ and $CeFe_2H_{3.75}$, previously published.[53] The decrease of the fine structure after hydridation reveals the presence of a strong feature at about 6 $Å^{-1}$ in the hydride derivative that has been already ascribed to the existence of a $2p4d \rightarrow (5d)^2$ transition.[49] In the case of crystalline $CeFe_2$ no clear evidence of such transition can be inferred from the spectrum because, if present, it is hidden by the strong EXAFS oscillations. However, it is possible to note that there is a discontinuity of the normal oscillating behavior of the EXAFS signal just centered at the same position where the double-electron transition occurs in the case of the hydride. This trend is associated with the fact that the double-electron resonance is located in one region where the EXAFS structure becomes negative. In fact, as shown in Fig. 7, if we subtract the $L_3N_{4,5}$ resonance taken directly from the hydride EXAFS spectrum, a "normal" oscillating trend for $CeFe_2$ EXAFS is recovered.

Once the double-electron excitation has been isolated it is possible to estimate how it modifies the conventional EXAFS data analysis. To this end, we have per-

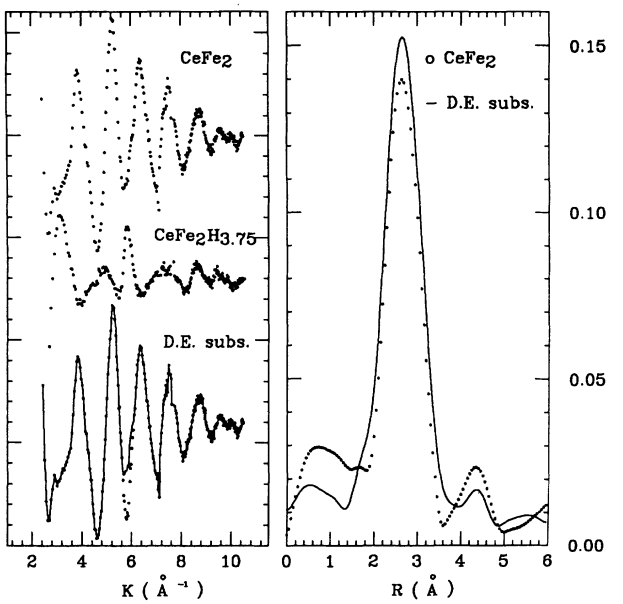

FIG. 7. Cerium L_3-edge EXAFS spectra in $CeFe_2$ and $CeFe_2H_{3.75}$ systems, taken from Ref. 53. The double-electron transition at 6 $Å^{-1}$ has been extracted from the hydride and subtracted to $CeFe_2$. The right panel shows the comparison between the Fourier transform before and after the subtraction.

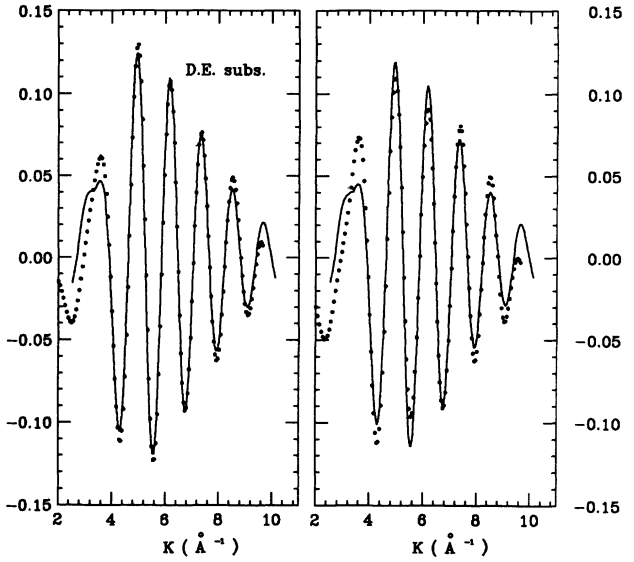

FIG. 8. Comparison between the experimental (dotted line) and calculated (solid line) EXAFS signals at the cerium L_3 in the case of $CeFe_2$ (left panel). In the right panel the same comparison is shown but when the double-electron transition has been subtracted. The experimental spectra were back-Fourier-transformed in the range 1.2–3.8 Å. The calculated signals correspond to the single-scattering contribution of 12 Fe atoms located at a distance of 3.03 Å away from the absorber Ce. The parameters used for the theoretical simulation are just the same in the two cases; only the coordination number has been allowed to vary.

formed a Fourier transform in the range 2.5–10.4 $Å^{-1}$ on a k-weighted EXAFS spectrum for both cases, i.e., with and without the $2p4d \rightarrow (5d)^2$ resonance. The result, shown in Fig. 7, indicates the presence of one unphysical structure at low R overlapping the first-shell contribution which disappears when the double excitation has been removed from the experimental spectrum, and at the same time, the height of the Fourier transform peaks is modified. This last effect clearly underlines the strong influence of multielectron excitations on structural analysis and, in particular, the effect on coordination number extraction. We have estimated it in the case of $CeFe_2$ by performing a theoretical simulation of the EXAFS spectrum using theoretical signals generated using the FEFF31 code,[67] to compare the experimental EXAFS spectrum to that where the double-electron feature has been previously removed. The theoretical EXAFS signal at the Ce L_3 edge was calculated for 12 Fe atoms located at 3.03 Å from the absorber Ce atom. The experimental spectra were back-Fourier-transformed in the range 1.2–3.8 Å. During the fit process the only parameters allowed to vary were the energy reference E_0 and the Debye-Waller factor. Best fits are shown in Fig. 8 where all the parameters used are the same for the two spectra. In the case of the original spectrum the coordination number is found to be lower by a 9% than the crystallographic one (12) meaning that the quality of the fit is clearly reduced as compared to the double-excitation subtracted spectrum.

IV. SUMMARY AND CONCLUSIONS

A systematic x-ray-absorption investigation was carried out in several rare-earth systems to verify the presence of double-electron resonances on the EXAFS spectra at the L edges of the rare earth. In all the systems investigated anomalous features, contributing in the EXAFS spectra far beyond the absorption edge, have been detected. These resonances are ascribed to the excitation of a secondary electron coming from a $4d$ level for both the L_3 and L_1 edges.

We have applied the result of the explicit computation of the relative cross sections for bound-state double-electron $LN_{4,5}$-edge transitions. These calculations were performed by using a many-body perturbation model that takes explicitly into account final state relaxation. It leads to the identification of all the allowed final states involved in the multielectron process, showing for the first time which transitions are expected to be observable.

Applying a deconvolution process to the experimental absorption spectra it is possible to extract the intensity of these multielectron features. The comparison between the calculated and observed resonances is quite straightforward. The influence of multielectron transitions on the EXAFS data analysis is shown to lead to a correction of about 10% on coordination numbers in the case of crystalline systems with no significant modification of

the interatomic distances. On the other hand, in the case of amorphous samples, the EXAFS signal is strongly distorted and it is not possible to extract any reliable structural information at all without previous subtraction of the multielectron resonances.

ACKNOWLEDGMENTS

We are indebted to T. Murata for valuable technical assistance during the experiments. We wish to thank O. Gzowski and Y.J. Lee for providing the samples. S. Stizza and M. Marziali are especially acknowledged for helping us in the preparation and characterization of the gel samples at CIGA (Centro Interdipartimentale Grandi Apparecchiature) of Camerino University. Valuable discussions with J. Purans and J. Garcia are recognized. One of us (J.Ch.) acknowledges an Spanish Ministerio de Educacion y Ciencia FPI grant. T.A.T. acknowledges support from the Standford School of Humanities and Sciences and the Dean of Research. This research project has been performed with the approval of the Photon Factory Program Advisory Committee (Proposal No. 92-295).

*Also at Department of Chemistry, Stanford University, California 94305.

[1]W. Wolfli, Ch. Stoller, G. Bonani, M. Suter, and M. Stockli, Phys. Rev. Lett. **35**, 690 (1975).
[2]G. Bradley Armen, T. Aberg, Kh. Rezul Karim, J.C. Levin, B. Crasemann, G.S. Brown, M.H. Chen, and G.E. Ice, Phys. Rev. Lett. **54**, 182 (1985).
[3]M. O. Krause and C. D. Caldwell, Phys. Rev. Lett. **59**, 2736 (1987).
[4]A. Li-Scholz, A. Leiberich, and W. Scholz, Phy. Rev. A **26**, 3232 (1982).
[5]R. D. Richtmyer, Phys. Rev. **49**, 1 (1936).
[6]L. C. Parrat, Phys. Rev. **49**, 132 (1936).
[7]R. D. Deslattes, Phys. Rev. **133**, 390 (1964).
[8]R. D. Deslattes, Phys. Rev. **133**, 399 (1964).
[9]T. A. Carlson, Phys. Rev. **156**, 142 (1967).
[10]M. O. Krause, T. A. Carlson, and R. D. Dismukes, Phys. Rev. A **170**, 37 (1968).
[11]T. A. Carlson and M. O. Krause, Phys. Rev. **140**, A1057 (1965).
[12]For a review V. Schmidt, Rep. Prog. Phys. **55**, 1483 (1992).
[13]G. Wentzel, Ann. Phys. (Leipzig) **66**, 437 (1921).
[14]M. J. Druyvestein, Z. Phys. **43**, 707 (1927).
[15]F.K. Richtmyer, J. Franklin Inst. **208**, 325 (1929).
[16]C. Bonelle and F. Wuilleumier, C.R. Acad. Sci. **256**, 5106 (1963).
[17]H. W. Schnopper, Phys. Rev. **131**, 2558 (1963).
[18]R. P. Madden and K. Codling, Phys. Rev. Lett. **10**, 516 (1963).
[19]F. Wuilleumier, J. Phys. (Paris) **26**, 776 (1965).
[20]K. Codling, R. P. Madden, and D. L. Ederer, Phys. Rev. **155**, 26 (1967).
[21]F. Wuilleumier and C. Bonnelle, C.R. Acad. Sci. Paris **270**, 1029 (1970).
[22]J. M. Esteva, B. Gauthe, P. Dhez, and R. C. Karnatak, J. Phys. B **16**, L263 (1983).
[23]A. Hiraya, K. Fukui, P.K. Tseng, T. Murata, and M. Watanabe, J. Phys. Soc. Jpn. **60**, 1824 (1991).
[24]R. D. Deslattes, Phys. Rev. **133**, 399 (1964).
[25]A. D. Deslattes, R. E. Lavilla, P. L. Cowen, and A. Henins, Phys. Rev. A **27**, 923 (1983).
[26]U. Kuetgens and J. Hormes, Phys. Rev. A **44**, 264 (1991).
[27]F. Wuilleumier, C.R. Acad. Sci. Paris **263**, 450 (1966).
[28]B.M. Kincaid and P. Eisenberger, Phys. Rev. Lett. **34**, 1361 (1975).
[29]M. Deutsch and M. Hart, Phys. Rev. A **34**, 5168 (1986).
[30]M. Deutsch and M. Hart, Phys. Rev. Lett. **57**, 1566 (1986).
[31]M. Deutsch and M. Hart, J. Phys. B **19**, L303 (1986).
[32]E. Bernieri and E. Burattini, Phys. Rev. A **35**, 3322 (1987).
[33]B. W. Holland, J.B. Pendry, R.F. Pettifer, and J. Bordas, J. Phys. C **11**, 633 (1978).
[34]M. Deutsch, G. Brill, and P. Kizler, Phys. Rev. A **43**, 2591 (1991).
[35]K. Zhang, E. A. Stern, J. J. Rehr, and F. Ellis, Phys. Rev. B **44**, 2030 (1991).
[36]M. Deutsch and M. Hart, Phys. Rev. A **29**, 2946 (1984).
[37]M. Deutsch, M. Hart, and P. Durham, J. Phys. B **17**, L395 (1984).
[38]S. I. Salem and B. Dev, Phys. Rev. A **22**, 2679 (1980).
[39]S. I. Salem, D. D. Little, A. Kumar, and P. L. Lee, Phys. Rev. A **24**, 1935 (1981).
[40]S. I. Salem, A. Kumar, and P. L. Lee, Phys. Lett. **92A**, 331 (1982).
[41]S. I. Salem and A. Kumar, J. Phys. B **19**, 73 (1986).
[42]S. I. Salem, A. Kumar, and P. L. Lee, Phys. Rev. A **25**, 2069 (1982).
[43]S. I. Salem, A. Kumar, K. G. Schiessel, and P. L. Lee, Phys. Rev. A **26**, 3334 (1982).
[44]A. Kumar, B. L. Scott, and S. I. Salem, J. Phys. B **18**, 3105 (1985).
[45]A. Kodre, M. Hribar, I. Arcon, D. Glavic-Cindro, M. Stuhec, R. Frahm, and W. Drube, Phys. Rev. A **45**, 4682 (1992).
[46]E. A. Stern, Phys. Rev. Lett. **49**, 1353 (1982).
[47]A. Bianconi, J. Garcia, M. Benfatto, A. Marcelli, C. R. Natoli, and M. F. R. Lopez, Phys. Rev. B **43**, 6885 (1991).
[48]A. Filipponi, E. Bernieri, and S. Mobilio, Phys. Rev. B **38**, 3298 (1988).
[49]J. Garcia, A. Marcelli, M. Sanchez del Rio, J. Bartolomè, D. Fruchart, S. Miraglia, and F. Vaillant, Physica B **158**, 521 (1989).
[50]S. Benazeth, M.H. Tullier, and M. Guittard, Physica B **158**, 39 (1989).
[51]M.H. Tullier, E.K. Hill, A. Tressaud, and B. Chevalier, in *Proceedings of the 2nd European Conference on Progress in X-Ray Synchrotron Radiation Research*, Bologna, 1990, edited by A. Balerna, E. Bernieri, and S. Mobilio (IPS, Bologna, 1990), Vol. 25, pp. 121–123.
[52]J. Chaboy, J. Garcia, J. Bartolomè, D. Fruchart, S. Miraglia, and A. Marcelli, in *Proceedings of the 2nd European Conference on Progress in X-Ray Synchrotron Radiation Research*, Bologna, 1990 (Ref. 51), pp. 77–780.
[53]J. Chaboy, J. Garcia, A. Marcelli, and M.F. Ruiz Lopez, Chem. Phys. Lett. **174**, 389 (1990).

[54]J. Chaboy, Ph.D. thesis, Zaragoza University, 1991.
[55]J. Chaboy, J. Garcia, A. Marcelli, and T.A. Tyson, Jpn. J. Appl. Phys. **32**, 61 (1993).
[56]J. Chaboy, J. Garcia, and A. Marcelli, Solid State Commun. **12**, 939 (1992).
[57]G. Li, F. Bridges, and G. S. Brown, Phys. Rev. Lett. **68**, 1609 (1992).
[58]M. Nomura, A. Koyama, and M. Sakurai (unpublished).
[59]S. Stizza, M. Marziali, O. Gzowski, J. Chaboy, A. Marcelli, and K. Szaniawska, Jpn. J. Appl. Phys. **32**, 797 (1993).
[60]U. Chung and J.Y. Lee, J. Non-Cryst. Solids **11**, 203 (1989).
[61]Y.G. Kim, S.M. Lee, and J.Y. Lee, J. Less-Common Met. **169**, 245 (1991).
[62]J.A. Victoreen, J. Appl. Phys. **19**, 855 (1948).
[63]J. Chaboy and T.A. Tyson, Phys. Rev. B **49**, 5869 (1994).
[64]T.A. Tyson, Ph.D. thesis, Stanford University, 1991.
[65]M. Ya Amusia and V.K. Ivanov, Usp. Fiz. Nauk **152**, 185 (1987) [Sov. Phys. Usp. **30**, 449 (1987)].
[66]J. Röhler, J. Magn. Magn. Mater. **47&48**, 175 (1985).
[67]J.J. Rehr, J. Mustre de Leon, S.I. Zabinsky, and R.C. Albers, J. Am. Chem. Soc. **113**, 5135 (1991).